Buoyancy-driven turbulent flow in particle-laden fluid subject to radiation

By R. Zamansky, F. Colletti, M. Massot AND A. Mani

1. Motivation and objectives

In turbulent fluid flows laden by particles or droplets, the velocity lagging of the dispersed phase can lead to high local concentration in zones of shear and away from vorticity cores (Squires & Eaton 1991). However, in isothermal non-reactive flows, the dispersed phase will only affect the velocity field if the loading is high and/or the particle size is comparable to the minimal flow scales (Crowe *et al.* 1996).

In several natural phenomena, turbulent dispersed multiphase flows occur under strong thermal radiation. In cloud physics, preferential concentration is believed to play an important role in determining the rate of droplet coalescence (Shaw 2003; Grabowski & Wang 2013). In circumstellar disks, turbulent clustering appears to be critical for the aggregation of chondrules and other constituents into primitive planetesimals (Cuzzi *et al.* 2001). Among the many industrial applications where radiation is coupled to particle-laden turbulence, examples are the injection of fuel sprays in combustion chambers (Vié *et al.* 2012; Watanabe *et al.* 2008) and aluminum particles in solid rocket motors (Doisneau *et al.* 2013; Duval *et al.* 2004).

In most previous studies turbulent agitation is enforced either by the inertia of the imposed flow velocity, or by a prescribed turbulent spectrum (Deshmukh *et al.* 2007; Matsuda *et al.* 2012). In the present contribution we explore a novel regime, in which the forcing is provided to the fluid by the radiation, through the dispersed phase. Specifically, we consider a large number of randomly distributed particles immersed in a transparent fluid, initially at rest and subject to thermal radiation (Fig. 1a). Non-uniformities in particle concentration result in local temperature variations due to the different absorptivity of the dispersed and carrier phases. Fluid motion is induced by gas expansion and (under the influence of an acceleration field) buoyancy, altering the particle distribution and potentially inducing higher non-uniformities. The coupling between local particle concentration, temperature fluctuations and hydrodynamic forcing is schematically illustrated in Fig. 1b. With respect to other dispersed multiphase flow problems, the main difference is the retroaction of the dispersed phase on the carrier fluid, which happens here through the thermal energy released in the fluid by conduction and convection.

Since the flow scales are not imposed a priori, but depend on the interplay between multiple phenomena, we perform a scaling analysis from which a set of relevant non-dimensional parameters is deduced. Direct numerical simulations are carried out using a pseudo-spectral method in a periodic cubic domain. Different scenarios associated to different particle concentration and properties, intensity of the radiation and size of the domain are considered. A number of simplifying assumptions are made, so that the problem is well defined and amenable to detailed calculations, still maintaining the essential features of more complex configurations. We show that the feedback loop depicted in Fig. 1b can trigger and sustain turbulence. The process is spontaneous and self-sustained in a large fraction of the parameter space.

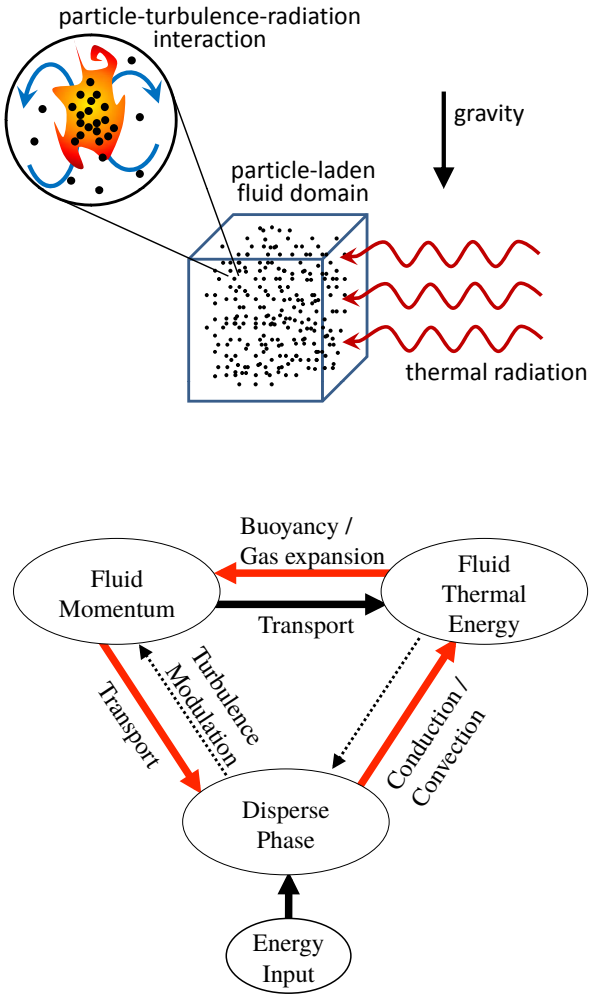

FIGURE 1. Flow configuration, with periodic boundary conditions (top). Scheme of the interplay between fluid momentum, fluid temperature and particles (bottom). The plain arrows represent the leading order interactions. The red arrows emphasize the feedback loop.

The report is organized as follows. In section 2 we formulate the basic assumptions and derive the spatial and temporal scales of the flow. In section 3 the non-dimensional form of the governing equations are presented. Section 4 gives the details of the numerical approach used. Section 5 demonstrates the strong coupling between fluid momentum, thermal energy and particle dispersion, with results that support the proposed scaling. In section 6 we draw the conclusions and present possible extension of the work.

2. Basic assumptions and typical scales

In order to retain the minimal physics for capturing the dynamics of the interaction between turbulent convection, temperature variation and particle dispersion, the following assumptions are considered:

(i) The radiative heat flux is constant and homogeneous, the carrier phase is transparent and the incident radiative flux on a particle is totally absorbed.

(ii) The particles are monodispersed spheres.

(iii) The particle concentration is low enough to neglect mutual particle interactions. both at short scales (particle collisions) and long scales (screening effect).

(iv) We focus on the low radiative flux regime. In this limit, the fluid density variation is small, and can be retained only in the buoyancy forcing term. For the same reason, the mean temperature of the system is considered as quasi-stationary over times relevant for the dynamics.

(v) The particles are in thermal equilibrium with the surrounding gas.

(vi) The Prandtl number Pr of the carrier phase is one.

(vii) The domain is spatially periodic.

Under these assumptions the main physical parameters are: the fluid viscosity ν, density ρ_f, specific heat capacity c_f, thermal diffusivity κ and thermal expansion coefficient α; the particle diameter d_p, density ρ_p, specific heat capacity c_p and mean concentration (number density) $\overline{n}$; the radiative heat flux density Φ, the gravitational acceleration g, and the periodicity of the spatial domain H.

We now deduce a set of non-dimensional parameters based on estimations of the characteristic temperature, length and time scales of the system. We focus on the relatively hot plume surrounding each particle (or clusters of particles). The scales are estimated by assuming a balance between inertia an buoyancy, and between heat production and dissipation in the vicinity of plume. Furthermore a small scale of the system, analogous to the Kolmogorov dissipative scale, is introduced to represent the scale of minimum heterogeneity.

Consistently with the assumptions (i) (ii) and (iii), the radiative heat flux received by one particle, Φ_p, is constant and equal to $\Phi_p = \dfrac{\pi}{4} d_p^2 \Phi$. Due to the constant heat supply, the temperature of the system rises steadily. The mean rate of fluid temperature increase β is

$$\beta = \frac{d\langle T \rangle_s}{dt} = \frac{\overline{n}\Phi_p}{\rho_f c_f} \ , \tag{2.1}$$

where T is the fluid temperature and $\langle \bullet \rangle_s$ stands for spatial averaging.

Since the particle preferential concentration plays a fundamental role in the above-mentioned coupling, we expect the particle Stokes number St, (i.e. the ratio of the particle response time, $\tau_p = \rho_p d_p^2 / \rho_f 18\nu$, to the time scale of the flow structures) to be a key parameter. However, unlike in "one-way-coupled" particle-laden flows, where the fluid flow is not influenced by the dispersed phase, here the flow time scale is not known *a priori*, but is the result of the interaction between the particle clusters and the plumes that surrounds them. To estimate the flow scales attached to the plume dynamics, it is firstly assumed that the effect of the viscosity is negligible (i.e. small velocity gradients). Therefore, in each plume the fluid inertia is balanced by the buoyancy forcing:

$$a_* = \frac{u_*}{t_*} \sim \alpha g \theta_* \ , \tag{2.2}$$

where θ_* and a_* are the typical plume temperature difference (with respect to the spatial average) and acceleration. The latter is expressed by the characteristic response time of the flow to the local heating t_*, and the characteristic convective velocity of a plume $u_* = \ell_* / t_*$ with ℓ_* a measure of the flow inhomogeneity, i.e., the typical distance between plumes. We remark that Eq. (2.2) is equivalent to the definition of Brunt-Väisälä

frequency (Borue & Orszag 1997): $t_* = \ell_*^{1/2} (\alpha g \theta_*)^{-1/2}$. Let us also assume that the temperature mixing in the vicinity of a plume is balanced by the heat released by the particles in this plume:

$$\varepsilon_\theta \sim \frac{\theta_*^2}{t_*} \sim \beta n_c' \theta_* \ , \tag{2.3}$$

where $\varepsilon_\theta = \kappa \sum_i \langle (\partial_i \theta)^2 \rangle$ is the temperature variance dissipation, and $n_c' = n_c / \overline{n}$ is the ratio of typical particle concentration in a cluster n_c to the mean particle concentration. The combination of Eq. (2.2) and (2.3) gives for t_* and θ_*

$$t_* = (\alpha g \beta n_c')^{-1/3} \ell_*^{1/3} \ , \tag{2.4}$$

$$\theta_* = (\alpha g)^{-1/3} (\beta n_c')^{2/3} \ell_*^{1/3} \ . \tag{2.5}$$

The distance between the particle clusters as well as the particle concentration in plumes are a priori highly fluctuating quantities, and dimensional analysis is not sufficient to estimate ℓ_* and n_c'. However, we can assume that at scales smaller than the dissipative scale of the system η, the viscous diffusion homogenizes the flow, and therfore $\ell_* \geq \eta$. The estimation of η is obtained from Kolmogorov scaling $\eta = \nu^{3/4} \varepsilon^{-1/4}$, where $\varepsilon = \nu \sum_{i,j} \langle (\partial_j u_i + \partial_i u_j)^2 \rangle$ is the mean turbulent kinetic energy dissipation. Subsequently ε is estimated by the turbulent kinetic energy budget in a plume: $\varepsilon_* = a_* u_*$ (i.e., Eq. (2.2) times u_*). This yields for η

$$\eta = \nu^{3/4} (\alpha g \beta \ell_*)^{-1/4} \, . \tag{2.6}$$

Equating the smallest scale of disturbance necessary to drive the flow out of mechanical equilibrium $\ell = \ell_{*,c}$ to η in Eq. (2.6) one obtains for $\ell_{*,c}$

$$\ell_{*,c} = \eta(\ell_{*,c}) = (\alpha g \beta)^{-1/5} \nu^{3/5}. \tag{2.7}$$

It should be noted that there is no influence of the heterogeneous particle distribution in this relation.

Due to the conservation of the total number of particle in the system, n_c and ℓ_* are connected through the geometry of the particle clustering. Without loss of generality n_c' is expressed as

$$n_c' = \left(\frac{\ell_*}{\ell_{*,c}} \right)^a \ , \tag{2.8}$$

where the exponent a as well as ℓ_* are unknown and depend in a non-trivial way on the fractal geometry of the particle cluster and the parameters of the flows. Recalling that $\ell_* \leq \ell_{*,c}$, relation (2.8) emphasizes that the particle repartition becomes homogeneous at scales smaller than $l_{*,c}$, whereas there are large regions of linear dimension ℓ_* which are almost devoid of particles. Inserting Eq. (2.8) in Eq. (2.4) and Eq. (2.5) and using Eq. (2.7), we obtain:

$$t_* \quad = (\alpha g \beta)^{-2/5} \nu^{1/5} \left(\frac{\ell_*}{\ell_{*,c}} \right)^{\frac{1-a}{3}} \quad = t_{*,c} \left(\frac{\ell_*}{\ell_{*,c}} \right)^{\frac{1-a}{3}} \ , \tag{2.9}$$

$$\theta_* = (\alpha g)^{-2/5} \beta^{3/5} \nu^{1/5} \left(\frac{\ell_*}{\ell_{*,c}} \right)^{\frac{1+2a}{3}} = \theta_{*,c} \left(\frac{\ell_*}{\ell_{*,c}} \right)^{\frac{1+2a}{3}} \ , \tag{2.10}$$

where we introduced $t_{*,c} = (\alpha g \beta)^{-2/5} \nu^{1/5}$ and $\theta_{*,c} = (\alpha g)^{-2/5} \beta^{3/5} \nu^{1/5}$ i.e. the time and temperature scales corresponding to the critical value $\ell_* = \ell_{*,c}$. We will assume that,

since the buoyancy forcing is directed vertically, the heterogeneity of the system is (to the first order) mono-dimensional. This assumption corresponds to $a = 1$, which allows dropping the dependence with n_c and ℓ_* in the expression for t_*: $t_* = t_{*,c}$.

In the limit of vanishingly small Stokes numbers, the particles are expected to be homogeneously distributed in the flow. Both n_c' and ℓ_* will present small fluctuations around their mean value: $n_c' \approx 1$ ($a = 0$) and $\ell_* \approx \overline{n}^{-1/3} = \overline{r_p}$. Here r_p represents the mean distance between neighbor particles. This gives for low inertia particles the following time and temperature scales, $t_{*,LI}$, $\theta_{*,LI}$

$$\frac{t_{*,LI}}{t_{*,c}} = \frac{\theta_{*,LI}}{\theta_{*,c}} = \left(\frac{\overline{r_p}}{\ell_{*,c}}\right)^{1/3} \quad . \tag{2.11}$$

Finally, the non-dimensional form of the set of parameters based on the critical scales $\ell_{*,c}$, $t_{*,c}$ and $\theta_{*,c}$ can be expressed as: the Stokes number $St = \dfrac{\tau_p}{t_{*,c}}$, the Reynolds number (or confinement parameter) $\gamma = \dfrac{H}{\ell_{*,c}}$, the density and heat capacity ratios ρ_p/ρ_f and c_p/c_f, the Prandtl number $Pr = \nu/\kappa$, the Froude number $Fr = \left(\dfrac{gt_{*,c}^2}{\ell_{*,c}}\right)^{-1/2}$ and the non-dimensional particle number density $C = \overline{n}\ell_{*,c}^3$.

The study focuses on the effect of the Stokes number, the particle concentration and the confinement scale, the other parameters being held constant. We expect to observe two different scaling behaviors, corresponding to either a fairly homogeneous particle distribution ($St \ll 1$ or $St \gg 1$) or highly segregated particles ($St = O(1)$).

3. Governing equations

We consider the limit of small domain size: $H \ll P_0/\rho_0 g$, small radiative power: $\beta \ll T_0/t_*$, and low Mach number, where quantities with 0 subscript denote reference thermodynamic quantity. Moreover, for time t sufficiently short ($t \ll T_0/\beta$), the temporal variation of the reference values is neglected and P_0, ρ_0 and T_0 are considered as quasi-stationary. Then following Spiegel & Veronis (1960), Dumont *et al.* (2002) or Shirgaonkar & Lele (2006), the full Navier Stokes system of equation simplifies according to the Oberbeck-Boussinesq approximation:

$$\nabla.\mathbf{u} = 0 \ , \qquad D_t\mathbf{u} = -\frac{1}{\rho_f}\nabla p + \nu\nabla^2\mathbf{u} + g\alpha\theta\mathbf{e_z} \ , \qquad D_t\theta = \kappa\nabla^2\theta + \frac{q'}{\rho_f c_f} \ , \tag{3.1}$$

where $D_t = \partial_t + \mathbf{u}.\nabla$, $\theta = T - T_0$ is the fluid temperature fluctuation around the reference temperature and $q' = q - \rho_f c_f \beta$ represents the spatial fluctuations of the thermal source term.

Concerning the expression of the thermal source term q in Eq. (3.1), since we neglect the short range perturbations around the particle (Boivin *et al.* 1998; Gatignol 1983; Maxey & Riley 1983), the influence of the particles is taken into account by Dirac distribution of the heat source term Φ_p.

$$q(\mathbf{x}) = \sum_p \Phi_p \delta(\mathbf{x} - \mathbf{x}_p) \ , \tag{3.2}$$

where $\mathbf{x}_p$ is the position of the pth particle and δ is the Dirac distribution. In the previous equation the heat flux exchanged between the particle p and the fluid is equal to the

radiative flux absorbed by the particle since we assumed that the particle is in thermal equilibrium with the fluid.

In the particle equation of motion, we only retain the Stokes drag and the gravitational force

$$d_t \mathbf{x}_p = \mathbf{u}_p \ , \qquad d_t \mathbf{u}_p = \frac{\mathbf{u} - \mathbf{u}_p}{\tau_p} + \left(1 - \frac{\rho_f}{\rho_p}\right) g \mathbf{e_z} \ , \tag{3.3}$$

with $\mathbf{u}_p$ the velocity of the particle p.

The non-dimensionnalization of Eq. (3.1)-(3.3) by scales $\theta_{*,c}$, $t_{*,c}$, $l_{*,c}$ and $u_{*,c} = l_{*,c}/t_{*,c}$ gives

$$\nabla.\mathbf{u} = 0 \ , \qquad D_t \mathbf{u} = -\nabla p + \nabla^2 \mathbf{u} + \theta \mathbf{e_z} \ , \qquad D_t \theta = \frac{1}{Pr} \nabla^2 \theta + c' \ , \tag{3.4}$$

$$d_t \mathbf{x}_p = \mathbf{u}_p \ , \qquad d_t \mathbf{u}_p = \frac{\mathbf{u} - \mathbf{u}_p}{St} + \frac{\mathbf{e_z}}{Fr^2} \ . \tag{3.5}$$

The thermal source term c' in Eq. (3.4) is expressed from Eq. (2.1) and (3.2) as the relative particle concentration: $c' = (\delta(\mathbf{x} - \mathbf{x}_p)/\overline{n}) - 1$. Note that the parameters γ and C are implicitly set by the size of the domain and the number of particles to be tracked.

4. Numerical simulations

Equations (3.4) are solved using a pseudo-spectral method (Canuto *et al.* 1988) in a periodic cubic domain of length 2π. The 2/3 rule is used for de-aliasing. The time integration is done by the second order Adams-Bashford method.

For the particle phase, we use Lagrangian tracking to obtain the evolution of the particle velocities and position. The gas velocity at the particle position is estimated from cubic spline interpolation (Garg *et al.* 2007). The time advancement for the particle equations also uses the second order Adams-Bashford algorithm, with the same time step as the flow.

The source term (3.2) is a Dirac distribution which needs to be projected onto the mesh. A local particle concentration field is obtain by regularization of the Dirac masses. Following Maxey *et al.* (1997) we choose to use a Gaussian shape regularization. This reads

$$\delta(\mathbf{x} - \mathbf{x}_p) \rightarrow c(\mathbf{x}, t) = A \ \exp\left(-\frac{(\mathbf{x} - \mathbf{x}_p)^2}{\sigma^2}\right) \ , \tag{4.1}$$

The regularization length σ should be independent of the mesh size $\Delta x = H/N$ (N^3 being the resolution). Therefore we chose σ to be commensurate to the smallest physical scale of the flow, i.e., $\sigma \approx \eta$, where the viscous scale of the flow can be estimated from Eq. (2.7). The Gaussian kernel (4.1) needs to be truncated to have a numerically efficient computation. The normalization parameter A is given by $A^{-1} = \int_{-k_2\sigma}^{+k_2\sigma} \exp\left(-\frac{(\mathbf{x}-\mathbf{x}_p)^2}{\sigma^2}\right) d\mathbf{x}$. In the present simulations we have choosen $k_1 = \sigma/\ell_{*,c} = 0.5$ and $k_2 = 3$ by comparing with other projection schemes (Garg *et al.* 2007).

The computational approach has been tested against the test cases reported by Maxey *et al.* (1997), which included decaying and forced homogeneous isotropic turbulence in the "one-way" and "two-way" coupling regimes. For brevity these comparisons are not presented in this report, but the agreement was satisfactory.

γ	C	N	N_p
82.9	1.82	128	$1.036\ 10^6$
82.9	0.35	128	$2.00\ 10^5$
82.9	0.19	128	$1.104\ 10^5$
50	0.35	64	$2.13\ 10^4$
218	0.35	256	$2.00\ 10^6$

TABLE 1. Parameters of the different simulations. All simulations, have been run for 7 Stokes numbers: $St = 0.003$, 0.019, 0.074, 0.352, 1.064, 7.343 and 29.36. For all cases, $Pr = 1$, $\rho_p/\rho = 909$ and $Fr = \infty$. N is the size of the mesh in each direction, N_p is the number of particles.

5. Results

5.1. *Numerical Parameters*

We inverstigate the effect of the particle inertia, mean number density and box size. To this end, we present a set of 63 simulations that have been run for 7 Stokes numbers (ranging from 3×10^{-3} to 30), 3 Reynolds numbers ($\gamma = 40$, 80, 220) and 3 mean particle concentrations ($C = 0.19$, 0.35 and 1.83), keeping all other parameters constant. In particular,we have imposed $1/Fr = 0$ (the direct effect of the gravity on the particle is negligible), $Pr = 1$ and $\rho_p/\rho_f = 909$. The parameters of the simulations are summarized in Table 1.

The number of particles in the simulations range from $N_p = 2.31 \cdot 10^4$ to $2.00 \cdot 10^6$ particles, in a domain of size $(2\pi)^3$ with computational mesh of 64^3, 128^3 or 256^3 elements. It has been checked *a posteriori* that, for the whole set of parameters, the mesh is sufficiently fine to properly resolve the smallest physical scale, *i. e.* $\Delta x < \eta$.

All simulations are initiated with quiescent flow conditions (zero velocity and temperature fluctuations) and particles randomly distributed in space.

5.2. *Evidence of the coupling and influence of the particle inertia*

Figure 2 presents snapshots of the fluid temperature and particle local concentration in the domain, for $St = 0.07$ and 0.3. In the former case the fields are fairly homogeneous, whereas in the latter, bulges of high temperature (the plumes) appear in correspondence with regions of high particle concentration (the clusters). At times, multiple bulges merge and create structures of size comparable with the size of the domain.

Figure 3 shows the temporal evolution of the turbulent kinetic energy in the box ($Tke = \frac{1}{2}\langle \mathbf{u}'.\mathbf{u}' \rangle_s$), for three Stokes numbers $St = 0.07$, 0.3 and 7.3. u' is the velocity fluctuation (note that due to the zero-divergence constraint and the periodic boundary conditions, $< u >_s = 0$). The turbulent kinetic energy is normalized by $u_{*,c} = \ell_{*,c}/t_{*,c}$ which is independent of the Stokes number (see Section 2). After an initial spin up ($t/t_* < 50$), the system reaches a statistical steady-state. The influence of the particle response time on the dynamics is clearly seen in this figure: at low Stokes numbers the system presents a low level of turbulent kinetic energy and correspondingly low fluctuations, while for higher Stokes numbers both the steady-state and the fluctuations level of the turbulent kinetic energy are significantly higher.

In Figure 4 we plot the distribution of the distance between neighboring particles, obtained from the computation of the Voronoï diagram (Monchaux *et al.* 2010). The PDFs are compared to the one for particles distributed according to the Poisson distri-

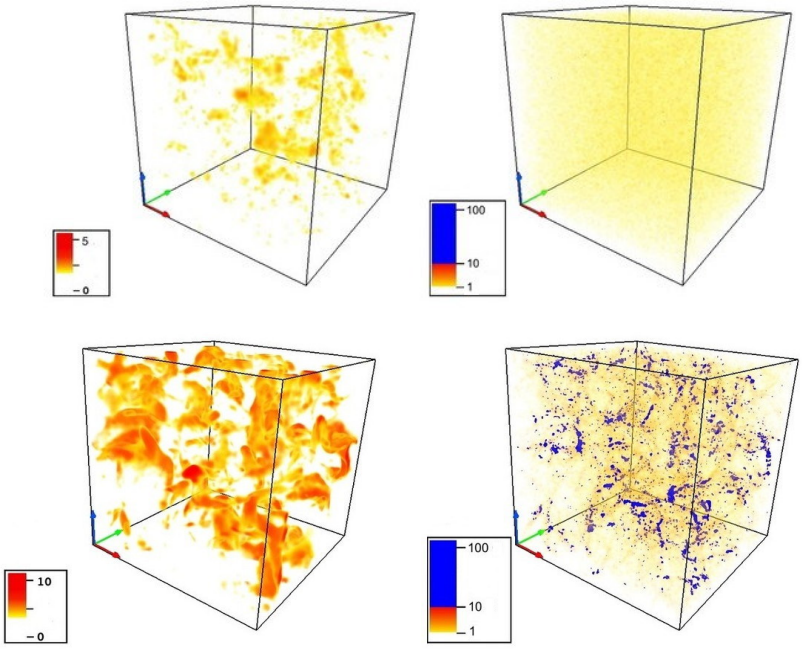

FIGURE 2. (a) and (b): snapshot for $\gamma = 80$, $St = 0.07$ and $C = 0.35$ of the positive fluid temperature fluctuations (colored by θ/θ_*) and particle concentration (colored by c'/C), respectively. (c) and (d): as in (a) and (b) for $\gamma = 80$, $St = 0.3$ and $C = 0.35$.

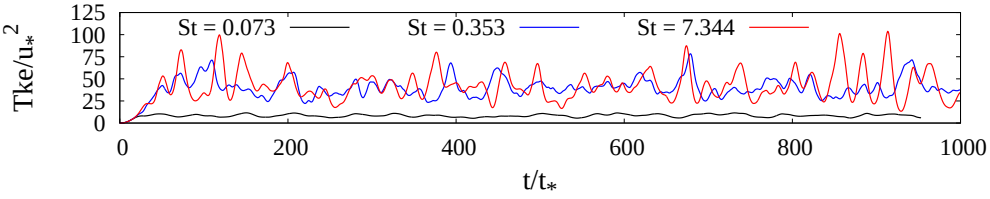

FIGURE 3. Time evolution of the turbulent kinetic energy for $St = 0.07$, 0.3 and 7.3, $\gamma = 80$ and $C = 0.35$.

bution (Ferenc & Néda 2007). For both high and low Stokes numbers ($St = 0.003$, 0.019 and 29.36), it is seen that the distribution of the inter-particle distance is very close to the one given by the Poisson distribution, and the particles are nearly homogeneously distributed. At $St = O(1)$ ($St = 0.074$, 0.352, 1.064, 7.343), the inter-particle distance distribution becomes much broader, which is the signature of intense particle clustering.

5.3. *Influence of the particle concentration*

In Figure 5, we plot the turbulent kinetic energy and turbulent dissipation rate versus the Stokes number, for three mean particle concentrations. The quantities presented in this figure have been spatially and temporally averaged (the initial transient dynamics is not taken into account) and are normalized by $u_{*,c}^2 = (\ell_{*,c}/t_{*,c})^2$ and $\varepsilon_{*,c} = \alpha g \theta_{*,c} u_{*,c}$, respectively. Note that both $u_{*,c}^2$ and $\varepsilon_{*,c}$ are independent of the Stokes number and depend on the mean concentration only through the definition of β (see Eq. 2.1). It

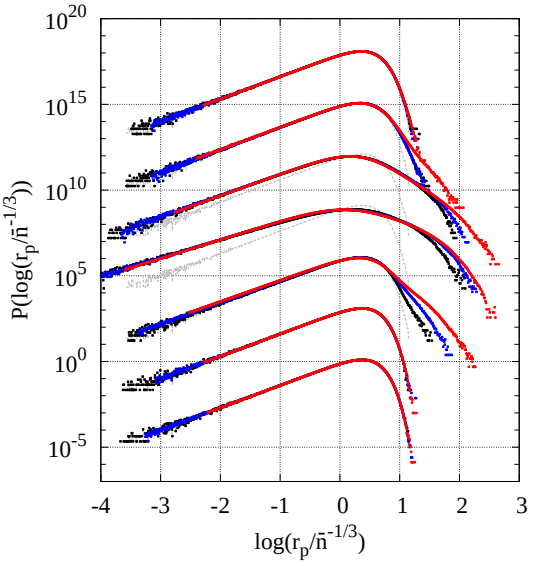

FIGURE 4. PDF of the logarithm of distance between pairs of neighbor particles as obtained from the Voronoï diagram, for $St = 0.003$, 0.019, 0.074, 0.352, 1.064, 7.343 and 29.36 (respectively shifted upward by 1000 units), for $\gamma = 40$ (black), 80 (blue) and 220 (red), and for $C = 0.35$. Comparision with the PDF corresponding to the Poisson distribution (in grey).

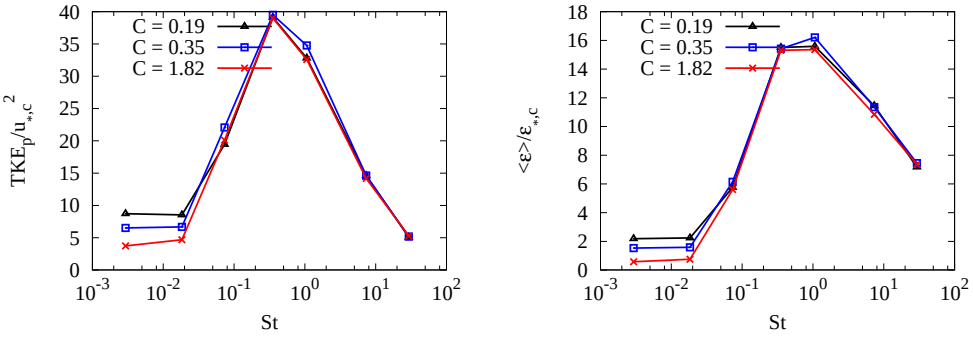

FIGURE 5. Evolution with the Stokes number of (a) the mean turbulent kinetic energy and (b) the mean turbulent kinetic energy dissipation, for three different mean particle concentration $C = 0.19$, 0.35 and 1.83 and $\gamma = 80$, normalized by the critical values $u^2_{*,c}$ and $\varepsilon_{*,c}$.

is seen that for sufficiently high Stokes numbers (say $St > 0.02$) there is no sizeable dependence on the particle concentration. It is also observed that both quantities peak around $St = O(1)$.

The dependency with the mean concentration observed for very low particle inertia indicates a qualitative change in the dynamical behavior of the system. When the particle response time becomes much smaller than any other scale of the flow, the scaling assumed in Eq. (2.11) applies. This is confirmed in Figure 6, where the turbulent kinetic energy and the dissipation are normalized by $u^2_{*,LI} = (\overline{n}^{-1/3}/t_{*,LI})^2$ and $\varepsilon_{*,LI} = \alpha g \theta_{*,LI} u_{*,LI}$. With such normalization scales, the quantities collapse for low Stokes numbers and are of order 1.

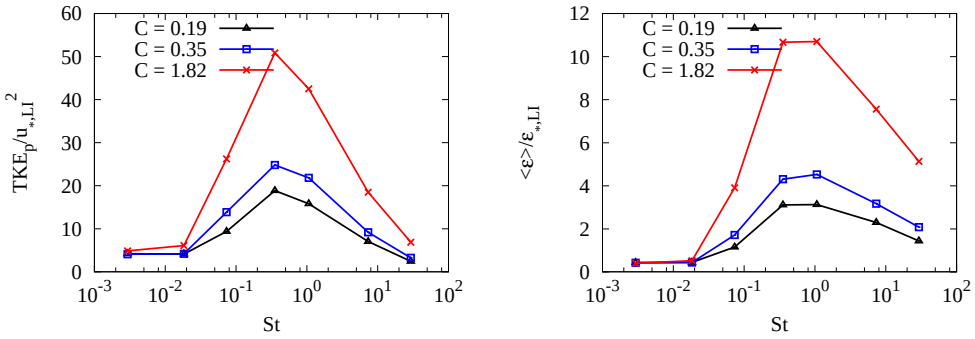

FIGURE 6. Evolution with the Stokes number of (a) the mean turbulent kinetic energy and (b) the mean turbulent kinetic energy dissipation, for three different mean particle concentration $C = 0.19$, 0.35 and 1.83 and $\gamma = 80$, normalized by the critical values $u^2_{*,LI}$ and $\varepsilon_{*,LI}$.

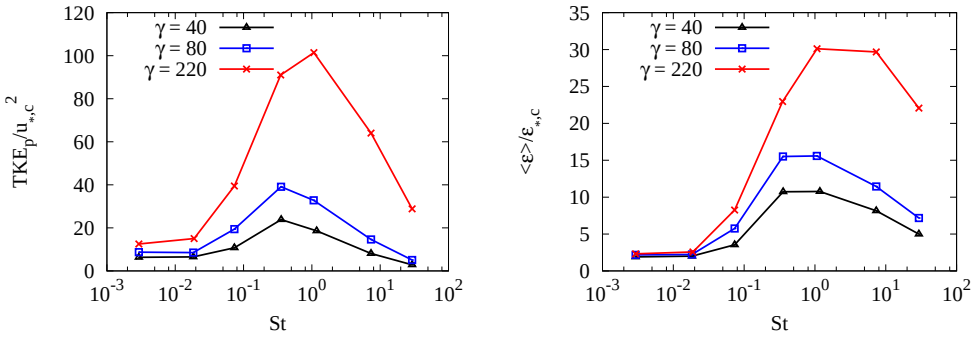

FIGURE 7. Evolution with the Stokes number of (a) the mean turbulent kinetic energy and (b) the mean turbulent kinetic energy dissipation, for three different confinement parameters $\gamma = 40$, 80, 220 and mean particle concentration $C = 0.35$, normalized by the critical values $u^2_{*,c}$ and $\varepsilon_{*,c}$.

This change in behavior indicates that when the particle inertia becomes commensurate with the typical time to set in motion the plumes, $t_{*,c}$ i.e. $St = O(1)$, the system is driven by the large fluctuations observed in the particle distribution and is not influenced by the mean particle concentration (all other parameters being constant).

5.4. *Influence of the domain size*

The domain size H imposes a specific maximum wavelength to the phenomenon. In order to investigate its effect, we show in Figure 7 the evolution of the turbulent kinetic energy and turbulent energy dissipation versus Stokes number for different values of the Reynolds number, keeping constant the mean particle concentration. As the St increases a strong influence of the confinement scale is observed. This indicates that for high enough Stokes numbers the preferential particle concentration becomes so important that the size of clusters and void regions are influenced by the domain size, as mentioned in section 5.2. Qualitatively similar collective dynamics have been observed in numerical simulations of particle settling (Guazzelli & Hinch 2011).

6. Conclusion

We have reported the first numerical simulation of interactions between particle-laden flow, radiation and buoyancy forcing. It has been observed that the buoyancy-induced fluid motion produces particle clustering, which enhances spatial and temporal temperature variations and leads to turbulent velocity fluctuations. This mechanism stimulates and enhances preferential concentration of the dispersed phase, and is therefore potentially relevant for natural phenomena in which agglomeration is critical, such as droplet growth in clouds and protoplanetary accretion. Preferential concentration by turbulence has long been considered a factor to explain high levels of segregation in such phenomena, but even so the accretion mechanism is not satisfactorily explained (Blum & Wurm 2008). Further research is warranted to verify whether the investigated coupling between radiation and particle transport is relevant in this sense.

The role of several parameters, which were kept constant in this study, needs to be further investigated. In particular, gravity has been considered here only as a source of buoyancy, without directly affecting the particles. The performed simulations display dependence with the domain size. While this could be an inherent property of the system, calculations on larger domains are planned to investigate this point. Finally, only relatively weak radiation levels have been considered. At higher intensities the fluid expansion might dominate on the buoyancy-driven motion.

Acknowledgments

M.M. wishes to thank Parviz Moin and the CTR at Stanford University for his hospitality and financial support during his sabbatical of Visiting Professor. The support of the France-Stanford Center for Interdisciplinary Studies through a collaborative project grant (PIs: P. Moin / M. Massot), is gratefully acknowledged.

REFERENCES

Blum, J. & Wurm, G. 2008 The growth mechanisms of macroscopic bodies in protoplanetary disks. *Ann. Rev. of Astronomy Astrophysics* **46**, 21–56.

Boivin, M., Simonin, O. & Squires, K. D. 1998 Direct numerical simulation of turbulence modulation by particles in isotropic turbulence. *J. Fluid Mech.* **375**, 235–263.

Borue, V. & Orszag, S. A. 1997 Turbulent convection driven by a constant temperature gradient. *Journal of Scientific computing* **12** (3).

Canuto, C., Hussaini, M., Quarteroni, A. & Zang, T. 1988 *Spectral Methods in Fluid Dynamics*. New York: Springer-Verlag.

Crowe, C. T., Troutt, T. R. & Chung, J. N. 1996 Numerical Models for Two-Phase Turbulent Flows. *Annual Review of Fluid Mechanics* **28** (1), 11–43.

Cuzzi, J. N., Hogan, R. C., Paque, J. & Dobrovolskis, A. 2001 Self-selective concentration of chondrules and other small particles in protoplanetary nebula turbulence. *Astrophys. J.* **546**, 496–508.

Deshmukh, K., Haworth, D. & Modest, M. 2007 Direct numerical simulation of turbulence-radiation interactions in homogeneous nonpremixed combustion systems. *Proceedings of the Combustion Institute* **31**, 1641–1648.

Doisneau, F., Laurent, F., Murrone, A., Dupays, J. & Massot, M. 2013 Eulerian

multi-fluid models for the simulation of dynamics and coalescence of particles in solid propellant combustion. *J. Comp. Phys.* **234**, 230 – 262.

Dumont, T., Genieys, S., Massot, M. & Volpert V. 2002 Interaction of Thermal Explosion and Natural Convection: Critical Conditions and New Oscillating Regimes. *SIAM J. App. Math.* **63,** (1), 351–372.

Duval, R., Soufiani, A. & Taine, J. 2004 Coupled radiation and turbulent multiphase flow in an aluminised solid propellant rocket engine. *J. Quant. Spectrosc. Radiat. Transfer* **84**, 513–526.

Ferenc, J.-S. & Néda, Z. 2007 On the size distribution of poisson voronoi cells. *Physica A* **385**, 518.

Garg, R., Narayanan, C. Lakehal, D. & Subramaniam, S. 2007 Accurate numerical estimation of interphase momentum transfer in Lagrangian-Eulerian simulations of dispersed two-phase flows. *Int. J. of Multiphase Flow* **33**, 1337–1364.

Gatignol, R. 1983 The Faxén formulae for a rigid particle in an unsteady non-uniform Stokes flow. *J. Méc. Theor. Appl.* **1**, 143.

Grabowski, W. W. & Wang, L.-P. 2013 Growth of cloud droplets in a turbulent environment. *Ann. Rev. Fluid Mech.* **45** (1).

Guazzelli, E. & Hinch, J. 2011 Fluctuations and Instability in Sedimentation. *Ann. Rev. Fluid Mech.* **43**, 97–116.

Matsuda, K., Onishi, R., Kurose, R. & Komori, S. 2012 Turbulence effect on cloud radiation. *Physical Review Letter* **108**, 224502.

Maxey, M. R., Pate, B. K., Chang, E. J. & Wang, L.-P. 1997 Simulations of dispersed turbulent multiphase flow. *Fluid Dynamics Research* **20**, 1–6.

Maxey, M. R. & Riley, J. J. 1983 Equation of motion for a small rigid sphere in a nonuniform flow. *Phys. Fluids* **26** (4), 883–889.

Monchaux, R., Bourgoin, M. & Cartellier, A. 2010 Preferential concentration of heavy particles: a Voronoi analysis. *Phys. Fluids* **22**, 103304.

Shaw, R. 2003 Particle-turbulence interactions in atmospheric clouds. *Ann. Rev. of Fluid Mech.* **35**, 183–227.

Shirgaonkar, A. A. & Lele, S. K. 2006 On the extension of the Boussinesq approximation for inertia dominated flows. *Phys. of Fluids* **18** (6), 066601.

Spiegel, E. A. & Veronis, G. 1960 On the Boussinesq approximation for a compressible fluid. *Astrophys. J.* **131**, 442.

Squires, K. D. & Eaton, J. K. 1991 Preferential concentration of particles by turbulence. *Phys. Fluids A* **3** (5), 1169–1178.

Vié, A., Jay, S., Cuenot, B. & Massot, M. 2012 Accounting for polydispersion in the eulerian large eddy simulation of the two-phase flow in an aeronautical-type burner. *Flow Turbul. Combust.* **In press** (Doi:10.1007/s10494-012-9440-x), 1–38.

Watanabe, H., Kurose, R., Komori, S. & Pitsch, H. 2008 Effects of radiation on spray flame characteristics and soot formation. *Combust. Flame* **152** (1-2), 2 – 13.